Composites Science and Technology 126 (2016) 122–129

Contents lists available at ScienceDirect

Composites Science and Technology

journal homepage: http://www.elsevier.com/locate/compscitech

Fracture toughness of polymeric particle nanocomposites: Evaluation of models performance using Bayesian method

Khader M. Hamdia [c, *], Xiaoying Zhuang [e, c], Pengfei He [f], Timon Rabczuk [a, b, c, d, **]

[a] Division of Computational Mechanics, Ton Duc Thang University, Ho Chi Minh City, Viet Nam
[b] Faculty of Civil Engineering, Ton Duc Thang University, Ho Chi Minh City, Viet Nam
[c] Institute of Structural Mechanics, Bauhaus-Universität Weimar, 99423 Weimar, Germany
[d] School of Civil, Environmental and Architectural Engineering, Korea University, Republic of Korea
[e] Department of Geotechnical Engineering, College of Civil Engineering, Tongji University, Shanghai, China
[f] School of Aerospace Engineering and Applied Mechanics, Tongji University, Shanghai, China

ARTICLE INFO

Article history:
Received 27 August 2015
Received in revised form
18 January 2016
Accepted 8 February 2016
Available online 15 February 2016

Keywords:
Nano particles
Fracture toughness
Modelling

ABSTRACT

This study presents a methodology to evaluate the performance of different models used in predicting the fracture toughness of polymeric particles nanocomposites. Three analytical models are considered: the model of Huang and Kinloch, the model of Williams, and the model of Quaresimin et al. The purpose behind this study is not to recommend which of the three models to be adopted, but to evaluate their performance with respect to experimental data. The Bayesian method is exploited for this purpose based on different reference measurements gained from the literature. The models' performance is compared and evaluated comprehensively accounting for the parameter and model uncertainties. Based on the approximated optimal parameter sets, the coefficients of variation of the model predictions to the measurements are compared for the three models. Finally, the model selection probability is obtained with respect to the different reference data.

1. Introduction

Polymeric nanocomposites (PNCs) are commonly formed by an epoxy matrix reinforced with a nanosized filler. Due to its inherent characteristic of high crosslink density, an epoxy polymer is known to be a relatively brittle material [1]. Nanofillers have shown great improvements in the physical and mechanical properties of epoxy-reinforced PNCs. Specifically, they have increased the fracture toughness compared to pristine epoxy. PNCs have numerous applications in nanotechnology such as: nano-biotechnology, nano-systems, nanoelectronics, and nano-structured materials. Generally, there are three categories of fillers: nanoparticles, nanoplatelet (layered), and nanofibrous materials. For this scale, the surface area - to - volume ratio is significantly large. Therefore, the composite properties are highly modified due to the extreme interfacial area between the nanofiller and the matrix [2]. Several experiments have been carried out in order to study the fracture behavior of polymer/particle nanocomposites ([3–12] among others). On the other hand, researchers developed numerical and analytical methods to get a better understanding of nanocomposite material behavior. A close form formula of energy dissipation due to the interfacial debonding between the particles and matrix was given by Chen et al. [13] considering the effect of particle sizes. Although, the increased fracture energy of rubber-toughened epoxy polymers was calculated by Huang and Kinloch [14], the model has been modified for PNCs by Refs. [7,8,10]. The improvement in the fracture toughness was attributed to two major mechanisms: localized plastic shear banding and debonding of silica nanoparticles. Further experimental studies also have implied this supposition [15–17]. According to the assumption of Williams [18], the energy dissipation is induced by the growth of plastic voids around debonded particles. The author concluded a large toughness increase for nanosize particles. Later, his work has been extended to cylindrical rods and fibres [19,20]. Quaresimin et al. [21] proposed a multiscale approach to predict the overall increase in the fracture toughness taking into account three different damage mechanisms: particle debonding, plastic yielding of nanovoids, and shear banding of the polymer. Based on experimental data gathered from the literature,

* Corresponding author.
** Corresponding author. Division of Computational Mechanics, Ton Duc Thang University, Ho Chi Minh City, Viet Nam
E-mail addresses: khader.hamdia@uni-weimar.de (K.M. Hamdia), timon.rabczuk@tdt.edu.vn (T. Rabczuk).

http://dx.doi.org/10.1016/j.compscitech.2016.02.012
0266-3538/

a stochastic approach has been presented to predict the fracture energy of PNCs by Ref. [22].

In general, all models inherently underlie an amount of uncertainties which can be related to the model itself and/or its input parameters. The former might be caused by the simplifications of the physical behavior, while the latter can be related to the number and the stochastic variance of the input parameters. Better predictions and the subsequent decrease in the model uncertainty are expected by introducing more factors in the model (increasing the model complexity). However, the parameters uncertainties become more dominant in this case. In light of this, the model with minimum total uncertainty is the most appropriate model, see Fig. 1 [23].

In recent years, Bayesian method has been introduced as an effective tool for evaluating models considering the model and parameters uncertainties based on measurements as reference data [24–27].

This paper is the first attempt to consider the model and parameters uncertainties in the assessment of the models used for the prediction of the fracture energy of PNCs. It aims at presenting a methodology to evaluate three different analytical models by using the Bayesian method. In particular, Huang and Kinloch model [14], Williams model [18], and the model according Quaresimin et al. [21] are examined. The purpose of the study is not to give a general recommendation which of the three model to use, but to evaluate their performance with respect to experimentally tested data series. The assessment is carried out based on different reference data (experimental measurements) gathered from the literature [3–12]. Nevertheless, the same methodology can be applied to evaluate the three models based on other measurements. The prior probabilities are first estimated considering the uncertainties in the parameters. Then we find the optimum parameter set which results in best fit of models prognoses and in consequence the coefficient of variation of the models predictions to the measurements are estimated. Eventually, the model selection probability is calculated.

The remainder of this paper is organized as follows. In Section 2, the considered models are briefly described. Section 3 presents the method for evaluating the models. Finally, the conclusion of this research is presented in Section 4.

2. Models for predicting the fracture properties of PNCs

Three existing models were chosen to be evaluated; the model of Huang and Kinloch [14], the model of Williams [18], and the model of Quaresimin et al. [21]. Hereafter, they are abbreviated by M_1, M_2, and M_3, respectively. These models have been selected due to their popularity and their applicability to different experimental studies. Moreover, they produce explicit predictions of the enhanced fracture energy of PNCs. Regarding the different theory and mechanism assumed, each of them has its own input parameters in addition to the joint parameters. Table 1 includes the definitions of the parameters and their stochastic variation. The uniform distribution was assumed for the parameters uncertainty. The upper and the lower limits of distributions were mostly proposed according to our previous studies [22,28].

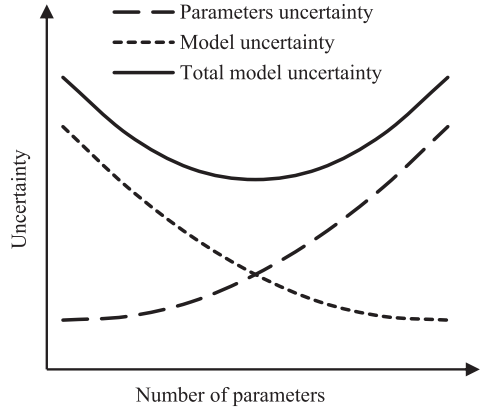

Fig. 1. Variation in model, parameter, and total uncertainties with respect to the number of parameters according to [23].

2.1. Huang and Kinloch

The model according to Huang and Kinloch [14] was first developed for the toughening mechanisms of rubber-modified epoxy polymers and more recently it has been modified for PNCs [7,8,10]. The localized plastic shear banding and debonding of nanoparticles which enable plastic void growth of the epoxy matrix are the two terms that taking part in the overall enhancement in the fracture toughness of PNCs, while rubber-bridging mechanism was disregarded. These two mechanisms are demonstrated in Fig. 2.

The improved fracture energy of PNCs, G_{Ic}, is expressed as

$$G_{Ic} = G_{Im} + \Delta G_s + \Delta G_v \tag{1}$$

where G_{Im} is the fracture energy of the matrix, and ΔG_s and ΔG_v are the contribution from the localized shear banding and the plastic void growth, respectively.

The term ΔG_s is given by

$$\Delta G_s = \frac{1}{2} V_f \sigma_{yc} \gamma_f F'(r_y) \tag{2}$$

where V_f is the volume fraction of the nano-filler, γ_{fm} is the matrix shear fracture strain, and σ_{yc} is the yield stress of the epoxy matrix under compression, which related to the tensile yield stress, σ_{ym}, by Ref. [5].

$$\sigma_{yc} = \sigma_{ym}\left(\frac{\sqrt{3}+\mu_m}{\sqrt{3}-\mu_m}\right) \tag{3}$$

μ_m is a material constant (pressure coefficient).

The parameter $F'(r_y)$ is a geometric term given by Ref. [15].

$$F'(r_y) = r_y\left[\left(\frac{4\pi}{3V_f}\right)^{1/3}\left(1-\frac{r_n}{r_y}\right)^3 - \frac{8}{5}\left(1-\frac{r_n}{r_y}\right)\left(\frac{r_n}{r_y}\right)^{5/2} - \frac{16}{35}\left(\frac{r_n}{r_y}\right)^{7/2} - 2\left(1-\frac{r_n}{r_y}\right)^2 + \frac{16}{35}\right] \tag{4}$$

where $r_n\,(=d_n/2)$ is the radius of nanoparticles and r_y is the radius of the plastic zone at the crack tip at fracture in the PNCs

$$r_y = \left(1+\frac{\mu_m}{\sqrt{3}}\right)^2 r_{ym} K_{vm}^2 \tag{5}$$

In Eq. (5), r_{ym} is radius of the plastic zone of the unmodified epoxy matrix estimated by Irwin's model [29] and K_{vm} is the maximum stress concentration factor of the von Mises stress in the matrix.

The term ΔG_v is calculated by

Table 1
The definitions of models' parameters.

Parameter	Symbol	Unit	Limits [lower,upper]	Models[a]
The volume fraction of the nano-filler	V_f	%	[0.5,10]	All
The average diameter of the nano-particles	d_n	nm	[10,80]	All
The elastic modulus (The Young's modulus) of the matrix	E_m	GPa	[2.4,3.6]	All
The fracture energy of the matrix	G_{Im}	J/m^2	[40,500]	All
The yield strength of the matrix	σ_{ym}	MPa	[70,120]	All
The Poisson's ratio of the matrix	ν_m	–	[0.33,0.37]	All
The shear fracture strain of the matrix	γ_{fm}	–	[0.70,0.75]	M_1,M_3
The pressure dependency material constant (pressure coefficient)	μ_m	–	[0.175,0.225]	M_1,M_3
The matrix maximum stress concentration factor of the von Mises stress	K_{vm}	–	[2.10,2.25]	M_1
The average diameter of voids around nanoparticles	d_v	nm	[25,120]	M_1
The percentage of the debonded particles	V_{dp}	%	[10,18]	M_1
The interfacial debonding energy	G_a	J/m^2	[0.01,1.5]	M_2,M_3
The shear yielding stress of the matrix	τ_{ym}	MPa	[40,70]	M_3
The thickness of the interphase	t	nm	[1,4]	M_3
The ratio of the shear elastic modulus of the interphase to the shear elastic modulus of the matrix	X	–	[0.1,2.0]	M_3

[a] M_1, M_2, and M_3 refer to Huang and Kinloch model, Williams model, and Quaresimin et al. model, respectively.

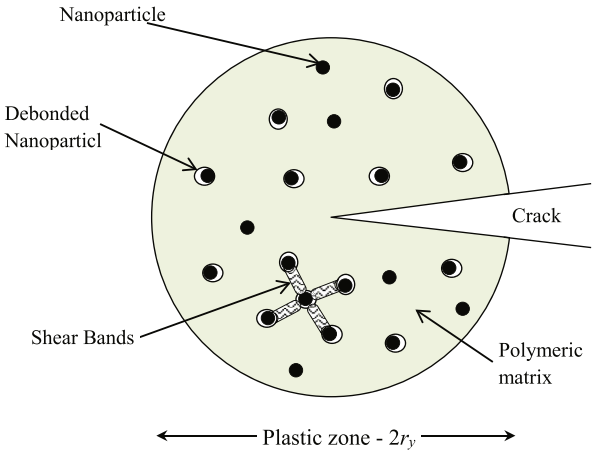

Fig. 2. Representative diagram for the toughening mechanisms of PNCs according to Huang and Kinloch [14].

$$\Delta G_v = \left(1 - \frac{\mu_m^2}{3}\right)\left(V_{fv} - V_{fp}\right)\sigma_{yc} r_{ym} K_{vm}^2 \tag{6}$$

where V_{fv} and V_{fp} are the volume fraction of voids and the volume fraction of debonded particles. An expression for $(V_{fv}-V_{fp})$ considering the average volume of the voids (v_v) and the average volume of nanoparticles (v_p) has been proposed by Refs. [8,10] as

$$\left(V_{fv} - V_{fp}\right) = \left(\frac{v_v}{v_p} - 1\right)V_{fp} \tag{7}$$

As reported in the studies of [7,17], not all of the nanoparticles have been observed to be debonded. Finite element simulations suggest that around 14% of the particles are debonded [17]. On this basis, we include a new factor to quantify the percentage of debonded particles (V_{dp}). It has been assumed to vary from 10% to 18%. The volume fraction of debonded particles, V_{fp} in Eq. (7), is substituted by $(V_{dp})(V_f)$

$$\left(V_{fv} - V_{fp}\right) = \left(\frac{v_v}{v_p} - 1\right)\left(V_{dp}\right)\left(V_f\right) \tag{8}$$

2.2. Williams

The analysis of Williams [18] has referred the energy dissipation to one basic mechanism; the debonding of nanoparticles which initiate the plastic void growth. At the first stage the rigid spherical nanoparticles is bonded to the surrounding matrix, and under tensile stress, the interfacial stress increases until debonding occur. This initiates the void growth in the matrix. The critical interfacial stress (debonding stress), σ_{cr}, is approximated by

$$\sigma_{cr} = \sqrt{\frac{4}{1+\nu_m}\frac{E_m G_a}{r_n}} \tag{9}$$

where G_a is the interfacial debonding energy, and ν_m is the Poisson's ratio of the matrix. If the number of the particles participating in the process is considered to be more than one, then the fracture energy of the PNCs is

$$G_{Ic} = G_{Im}\left(X_t V_f - 1.21 V_f^{2/3} + 1\right) \tag{10}$$

where X_t is toughening factor that is characterized by a critical stress ratio factor, x [18].

Both factors are given by

$$x = \frac{\sigma_{cr}}{\sigma_{ym}}\left[\frac{1+\nu_m}{2(1-\nu_m)}\right], X_t = \frac{(1+\nu_m)^2}{2\pi(1-\nu_m)}\left[\frac{e^{(x-1)}}{x} - \frac{5\nu_m - 1}{2(1+\nu_m)}\right] \tag{11}$$

2.3. Quaresimin et al.

A multiscale methodology has been adopted by Quaresimin et al. [21] to describe the toughening mechanism of PNCs. The authors have considered the interphase zone surrounding the nanoparticle to account for the interactions between the nanoparticles and the matrix. The adjacent polymer chains are disordered due the addition of the nanofiller, leading to the formation of interphase zones surrounding the nanoparticles with properties different from that of the bulk matrix. The extent of the impact of particle/polymer interface is principally influenced by the manufacturing techniques and the curing processes. The influence of the interphase was studied experimentally by Refs. [30–33] and numerically by Refs. [34–37]. Other advanced computational multiscale methods for crack propagation and material failure were

proposed for instance in Refs. [46-50].

Through its thickness, the interphase layer was assumed to be homogeneous and isotropic [38]. Fig. 3 displays the system considered at the nanosized scale.

By studying the energy dissipation at the nanoscale, Quaresimin and co-workers indicated that the overall fracture toughness of the nanocomposite is composed of three damaging mechanisms: (i) particle debonding, (ii) plastic yielding of nanovoids, and (iii) shear banding of the polymer [38–40].

The term of toughness improvement due to the debonding of nanoparticle is expressed by

$$\Psi_{dp} = \frac{2G_a}{3\pi r_n}\left(\frac{1+\nu_c}{1-\nu_c}\right)\left(\frac{E_c}{\sigma_{cr}^2 C_h^2}\right) \tag{12}$$

ν_c and E_c being the Poisson's ratio and the elastic modulus of the nanocomposite, respectively. In this study, ν_c was set equal to the matrix Poisson's ratio, ν_m, while E_c was calculated by the Hashin-Shtrikman solution developed in Ref. [41]. The debonding stress, σ_{cr}, and the reciprocal of the hydrostatic part of the global stress concentration tensor, C_h, depend on the nanoparticle radius, the interphase thickness, and the matrix and interphase elastic properties [38].

The part of the fracture toughness enhancement caused by the plastic yielding of nanovoids is [39].

$$\Psi_{py} = \frac{4}{9\pi C_h}\frac{E_c}{E_m}\frac{(1+\nu_c)(1+\nu_m)}{1-\nu_c}\frac{\sigma_{ym}}{\sigma_{cr}}\left(\frac{a}{r_n}\right)^{3\left(1-\frac{\sigma_{ya}}{\sigma_{ym}}\right)} e^{\left(3C_h\frac{\sigma_{cr}}{\sigma_{ym}}-1\right)} \tag{13}$$

where σ_{ya} is the yield stress of the interphase, and a is the external interphase radius (see Fig. 3).

The third part, the improvement due to the formation of localised plastic shear bands, is

$$\Psi_{SB} = \frac{I_{SB}}{4\pi\sigma_{yca}^2\left(1-\mu_m/\sqrt{3}\right)^2}\frac{E_c}{1-\nu_c^2}\Gamma \tag{14}$$

I_{SB} is referring to the stress concentration around the nanoparticles, σ_{yca} being the interphase yielding stress under compression, and Γ is quantifying the energy produced at the nanoscale. The shear yielding stress of the matrix, τ_{ym}, in addition to V_f, γ_{fm}, a, and r_n are required to calculate Γ, while I_{SB} is a function of ν_c, μ_m, C_h, and H_{vM} (the deviatoric component of the global stress concentration tensor) [40].

Eventually, the total fracture energy of PNCs is calculated by

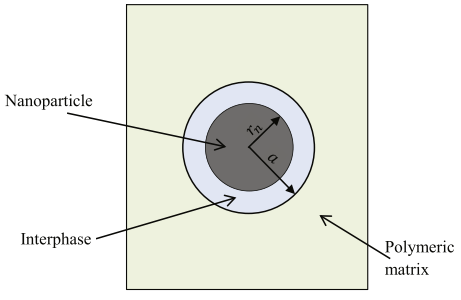

Fig. 3. 2D representation of the nanoscale system considered according to Quaresimin et al. [21].

$$G_{Ic} = \frac{G_{Im}}{1 - V_f\left(\Psi_{dp} + \Psi_{py} + \Psi_{SB}\right)} \tag{15}$$

The condition: $V_f(\Psi_{dp} + \Psi_{py} + \Psi_{SB}) < 1$, is essential for the applicability of the model in Eq. (15). Other values will produce meaningless results. This limits the applicability of the model in determining the fracture energy of PNCs reinforced by small fractions of nanofiller.

2.4. Discussion

Although, the model of Huang and Kinloch [14] accounts for the main damaging mechanisms, it is based on some simplifying assumptions. The knowledge of the increased volume fraction of voids (V_{fv}–V_{fp}) is required to evaluate the energy contribution from void-growth mechanism, ΔG_v (see Eq. (6)). The values for the volume fraction of voids, V_{fv}, and the volume fraction of debonded particles, V_{fp}, can be measured experimentally using for instance electron micrographs. Instead, based on the expression proposed in Refs. [8,10], we introduced a new uncertain parameter to quantify the percentage of debonded particles (V_{dp}). The proposed formula for (V_{fv}–V_{fp}) is shown in Eq. (8).

On the other hand, the model of Williams [18] assumes that the void growth around debonded particles is the only dominant energy dissipation mechanism. His analysis was based on the energy balance concept around a single nanoparticle and assuming the absence of particle-to-particle interaction. In turn, the effect of aggregation was ignored. A similar assumption, i.e. the absence of particle-to-particle interaction, was considered in the model of Quaresimin et al. [21]. However, three damaging mechanisms through multiscale modelling and the effect of the interphase zone were taken into account.

It is widely acknowledged that the nanofillers intend to agglomerate in nanocomposites. This may limit the applicability of the models of Williams [18] and Quaresimin et al. [21] to PNCs with a low volume fraction of fillers. However, since the most important merit of the PNCs is substantial improvements in the fracture toughness at low filler content, this is not a short-coming of the above mentioned models.

3. Assessment of PNCs fracture models using Bayesian method

The Model selection refers to the problem of selecting one model from a list of candidate models based on available data. The Bayes' rule of statistics has motivated [42] to develop the Bayesian approach for model selection by incorporating the different sources of uncertainties based on response measurements (reference data), D. The model selection probability is represented by the conditional probability of the model M_i given the reference data D. It can be calculated by

$$P(M_i|D) = \frac{P(D|M_i)P(M_i)}{\sum_i P(D|M_i)P(M_i)} \tag{16}$$

where $P(M_i)$ is the prior probability of M_i which is based on the user's judgment on the initial plausibility of the models. The data-dependent term $P(D|M_i)$ is the evidence of M_i. It defines the probability that the measurements of reference data D being represented by the predictions of the model M_i. Making use of the theorem of total probability, the evidence can be calculated by Ref. [42].

$$P(D|M_i) = \int P(D|X_i, M_i)P(X_i|M_i)dX_i \tag{17}$$

where $P(D|X_i, M_i)$ is the likelihood function and $P(X_i|M_i)$ is the prior probability of the input parameters.

The likelihood is the joint conditional probability of the reference data, D, given the input parameters, X_i. It measures how the model fit the data. A higher likelihood factor corresponds to better fit of M_i to D. The prior probability of the input parameters characterizes what is known about the parameters before any actual observation or modelling being considered. In the presence of measurements and model predictions, the prior probability is updated to posterior probability [43].

Assuming that the posterior probability of the parameters is approximated by a Gaussian distribution, the Laplace's method for asymptotic approximation can be applied to estimate the evidence as [44].

$$P(D|M_i) = P\left(D|\hat{X}_i, M_i\right)P\left(\hat{X}_i|M_i\right)\left[\left|H(\hat{X}_i)/2\pi\right|\right]^{-\frac{1}{2}} \tag{18}$$

where $\hat{X}_i$ is the optimal parameter set that maximize the posterior probability and $H(\hat{X}_i)$ is the Hessian matrix of $-\ln[P(D|X_i, M_i)P(X_i|M_i)]$ with respect to X_i calculated at $\hat{X}_i$. The models are compared according to their model selection probability calculated in Eq. (16). The model with the largest probability is the optimum one.

In the present work, the models of predicting the fracture energy of PNCs were evaluated. We considered the model of Huang and Kinloch [14] (M_1), the model of Williams [18] (M_2), and the model of Quaresimin et al. [21] (M_3), which were described in Section 2. The prior probabilities of these models were assumed to be equal, i.e. $P(M_1) = P(M_2) = P(M_3) = 1/3$.

Thanks to the uniform distribution assumed for the input parameters, the prior probabilities of the model parameters, $P(X_i|M_i)$, are constant disregarding the value of the parameter. The input parameters V_f, d_n, E_m, and G_{Im} were fixed as deterministic parameters, while we calculated the most probable value (optimal parameter value), which realized the best fit of the model predictions to the measurements, for the remaining parameters. Different experimental measurements gathered from the literature [3–12] have been utilized as reference data. For each, Table 2 shows the values of the calculated optimal parameter set.

Interestingly, the incorporation of the parameter V_{dp} in M_1 has enhanced the model predictions to fit the measurements. By the finite-element analysis of [45], the value of the maximum stress concentration for the von Mises stresses around a void, K_{vm}, was estimated to be 2.22 for a matrix of elastic modulus equal 3.2 GPa which agrees well with the optimal values obtained in this study. The interfacial debonding energy, G_a increases as the diameter of the nanofiller increases. Its optimal values were in the range of [0.184,1.360] and [0.010,0.046] for M_2 and M_3, respectively. Similar values of G_a for M_2 were reported in Refs. [18] and [20]. The high value of these results may be explained by assuming that the optimal values of G_a were reduplicated since the total energy dissipation in M_2 was attributed only to one mechanism. Based on this, the probability distribution of G_a can be updated to a uniform distribution in the range of [0.1,1.5] for M_2 and [0.01,0.1] for M_3. The elastic property of the interphase was softer than that of the matrix in the measurements; D_{10} and D_{11} (χ=1.162 and 1.231, respectively), whereas the matrix showed stiffer elasticity in the remaining measurements.

Exploiting the optimal parameter sets, the models predictions versus the nanofiller volume fraction are depicted in Fig. 4. Obviously, M_2 and M_3 mostly have a similar ascending trend but it differs slightly from M_1.

The model uncertainty can be demonstrated by the differences between the predictions and the measurements. This uncertainty is measured by the coefficient of variation (CV).

$$CV_{ij} = \frac{1}{\overline{D_j}}\sqrt{\frac{1}{N_j - 1}\sum_{m=1}^{N_j}(D_m - Y_{im})^2} \tag{19}$$

where $\overline{D_j}$ and N_j are the mean value and the number of the individual experiments of the j reference data, D_m is the measured value, and Y_{im} is the corresponding predicted value of the model M_i.

The CV values for M_1, M_2, and M_3 are shown in Fig. 5. Except of the measurements: D_8, D_{11}, D_{12}, and D_{13}, M_1 shows better performance compared to M_2 and M_3, where its CV values are the least. The predictions of M_2 have the lowest discrepancies from the measurements of D_{11}, D_{12}, and D_{13}. M_3 produces the best fit

Table 2
The values of the input parameters used in the assessment of the models.

Reference	All models[a]		M_1[b]							M_2[b]			M_3[b]							
Data	d_n	E_m	σ_{ym}	ν_m	γ_{fm}	μ_m	K_{vm}	d_v	V_{dp}	σ_{ym}	ν_m	G_a	σ_{ym}	ν_m	G_a	γ_{fm}	μ_m	τ_{ym}	t	χ
	nm	GPa	MPa	–	–	–	–	nm	%	MPa	–	J/m^2	MPa	–	J/m^2	–	–	MPa	nm	–
D_1 [3]	20	3.20	71.6	0.35	0.732	0.194	2.227	37.7	14.1	72.3	0.36	0.287	85.1	0.36	0.015	0.722	0.184	66.0	3.00	0.882
D_2 [3]	20	3.20	115.8	0.36	0.740	0.203	2.216	43.5	11.4	80.0	0.36	0.309	77.6	0.35	0.011	0.746	0.197	52.9	2.26	0.788
D_3 [4]	12	3.53	80.5	0.33	0.728	0.206	2.236	25.5	10.4	76.9	0.36	0.184	81.4	0.34	0.013	0.730	0.204	67.3	2.24	0.644
D_4 [4]	20	3.53	107.1	0.34	0.730	0.192	2.180	25.5	10.3	86.5	0.36	0.289	110.4	0.34	0.016	0.747	0.184	69.6	1.95	0.670
D_5 [4]	40	3.53	118.4	0.34	0.704	0.177	2.108	45.0	13.2	82.7	0.36	0.473	97.0	0.36	0.015	0.727	0.214	59.0	2.90	0.375
D_6 [5]	23	3.50	71.6	0.34	0.715	0.210	2.244	25.1	10.8	75.8	0.36	0.250	117.5	0.36	0.010	0.727	0.189	65.1	2.7	0.742
D_7 [5]	74	3.50	71.6	0.37	0.745	0.222	2.236	91.2	15.2	75.8	0.35	0.914	110.1	0.34	0.046	0.727	0.188	63.4	2.18	0.447
D_8 [6]	20	2.86	118.6	0.34	0.704	0.191	2.110	47.4	16.4	81.7	0.35	0.374	87.2	0.33	0.018	0.713	0.184	68.5	2.97	0.710
D_9 [7]	20	2.96	70.5	0.36	0.737	0.205	2.190	25.7	12.5	80.2	0.35	0.310	112.5	0.36	0.011	0.745	0.192	62.6	1.08	0.758
D_{10} [8]	20	2.41	70.3	0.35	0.747	0.208	2.224	42.2	14.1	73.5	0.36	0.363	94.8	0.35	0.011	0.710	0.187	67.3	1.32	1.162
D_{11} [8]	80	2.41	70.7	0.36	0.730	0.223	2.239	118.8	17.9	71.5	0.37	1.360	88.5	0.34	0.046	0.716	0.184	63.8	1.20	1.231
D_{12} [9]	25	3.02	118.4	0.34	0.704	0.177	2.108	29.8	13.3	81.8	0.34	0.340	109.6	0.34	0.012	0.734	0.203	48.3	3.91	0.676
D_{13} [9]	25	2.78	116.7	0.36	0.704	0.181	2.112	56.6	16.7	72.7	0.34	0.383	87.2	0.34	0.010	0.709	0.220	60.2	3.78	0.656
D_{14} [10]	20	2.96	71.5	0.37	0.741	0.222	2.229	42.0	13.7	77.4	0.33	0.385	79.0	0.36	0.011	0.708	0.185	50.8	3.43	0.649
D_{15} [11]	13	2.60	80.6	0.36	0.705	0.181	2.221	35.3	11.1	71.1	0.35	0.224	97.1	0.36	0.010	0.749	0.176	67.4	2.83	0.770
D_{16} [12]	25	3.27	117.1	0.33	0.708	0.185	2.204	36.4	14.9	83.5	0.36	0.322	110.0	0.36	0.011	0.731	0.215	46.4	3.89	0.830

[a] The values of d_n and E_m are obtained from the corresponding references.
[b] These are the optimal values approximated in the current study.

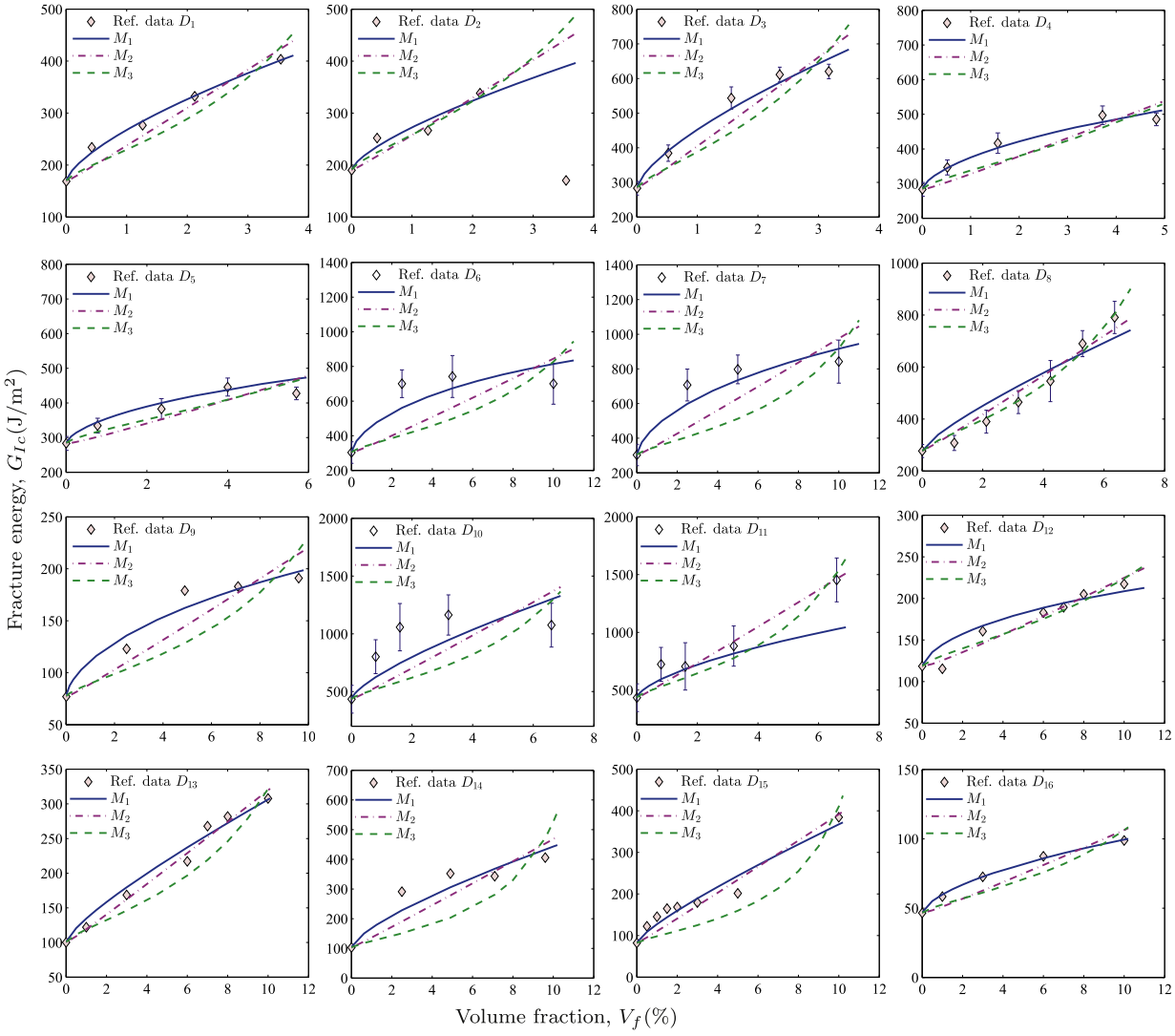

Fig. 4. Predictions of the models using the optimal parameter set for the different reference data.

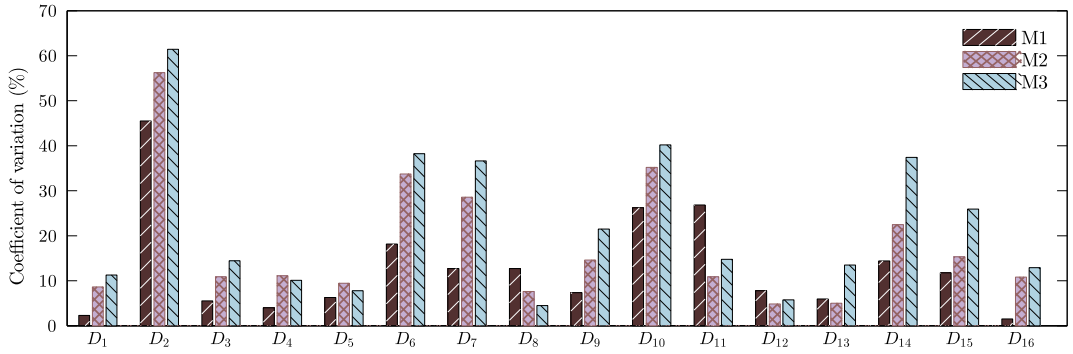

Fig. 5. The coefficient of variation for the different references data.

predictions in the measurements of D_8 only.

When considering both the model and parameters uncertainties in the evaluation, M_1 outperforms M_2 and M_3 for all the different measurements. It has significantly higher model selection probability, $P(M_i|D)$ (See Table 3). It can be concluded that the parameters of M_2 and M_3 have steeper posterior probabilities. Significant changes in their prognoses are expected due to slight variations in the parameters values. One possible explanation is that the natural exponential relation in M_2 and in M_3 results in high values of the determinant of their Hessian matrices.

Table 3
The models selection probability values for the different reference data.

Reference		$P(M_i\|D)$[a]		
Data		M_1	M_2	M_3
D_1	[3]	0.988	0.000	0.012
D_2	[3]	1.000	0.000	0.000
D_3	[4]	1.000	0.000	0.000
D_4	[4]	1.000	0.000	0.000
D_5	[4]	0.805	0.000	0.195
D_6	[5]	0.999	0.000	0.001
D_7	[5]	0.998	0.000	0.002
D_8	[6]	0.998	0.000	0.002
D_9	[7]	1.000	0.000	0.000
D_{10}	[8]	0.995	0.000	0.005
D_{11}	[8]	0.744	0.001	0.255
D_{12}	[9]	1.000	0.000	0.000
D_{13}	[9]	1.000	0.000	0.000
D_{14}	[10]	1.000	0.000	0.000
D_{15}	[11]	1.000	0.000	0.000
D_{16}	[12]	0.997	0.000	0.003

[a] The probability of selecting the model M_i given the different reference data calculated by Eq. (16).

4. Conclusion

Three existing models used for the prediction of the fracture toughness of PNCs were evaluated. The Bayesian method was employed to quantify the model selection probabilities of Huang and Kinloch [14] model, Williams [18] model, and Quaresimin et al. [21] model. The model and parameters uncertainties were considered in the assessment based on the experimental measurements of [3–12]. The optimal models predictions with respect to these measurements were obtained using the optimal parameter sets. In contradiction to the references data of D_8, D_{11}, D_{12}, and D_{13}, the optimal predictions of Huang and Kinloch model showed better performance compared the other two models. However, for all the reference measurements, the model of Huang and Kinloch showed a distinctly higher model selection probability. On this base, we can conclude that it is the most robust model with regard to the applied reference measurements.

Acknowledgement

The authors gratefully acknowledge the support for this research provided by the IRSES-MULTIFRAC and the Alexander von Humboldt Foundation in the framework of the Sofja Kovalevskaja Award endowed by the Federal Ministry of Education and Research, Germany. Dr. Xiaoying Zhuang thanks the National High-end Foreign Experts by State Administration of Foreign Experts Affairs, PRC of Tongji University.

Appendix A. Supplementary data

Supplementary data related to this article can be found at http://dx.doi.org/10.1016/j.compscitech.2016.02.012.

References

[1] A. Argon, R. Cohen, Toughenability of polymers, Polymer 44 (19) (2003) 6013–6032.
[2] E.T. Thostenson, C. Li, T.W. Chou, Nanocomposites in context, Compos. Sci. Technol. 65 (3) (2005) 491–516, http://dx.doi.org/10.1016/j.compscitech.2004.11.003.
[3] M. Zappalorto, A. Pontefisso, A. Fabrizi, M. Quaresimin, Mechanical behaviour of epoxy/silica nanocomposites: experiments and modelling, Compos. Part A Appl. Sci. Manuf. 72 (2015) 58–64.
[4] M. Zamanian, M. Mortezaei, B. Salehnia, J. Jam, Fracture toughness of epoxy polymer modified with nanosilica particles: particle size effect, Eng. Fract. Mech. 97 (2013) 193–206.
[5] P. Dittanet, R.A. Pearson, Effect of silica nanoparticle size on toughening mechanisms of filled epoxy, Polymer 53 (9) (2012) 1890–1905.
[6] H.Y. Liu, G.T. Wang, Y.W. Mai, Y. Zeng, On fracture toughness of nano-particle modified epoxy, Compos. Part B Eng. 42 (8) (2011) 2170–2175.
[7] T. Hsieh, A. Kinloch, K. Masania, J.S. Lee, A. Taylor, S. Sprenger, The toughness of epoxy polymers and fibre composites modified with rubber microparticles and silica nanoparticles, J. Mater. Sci. 45 (5) (2010a) 1193–1210.
[8] Y. Liang, R. Pearson, Toughening mechanisms in epoxy–silica nanocomposites (ESNs), Polymer 50 (20) (2009) 4895–4905.
[9] H. Zhang, L.C. Tang, Z. Zhang, K. Friedrich, S. Sprenger, Fracture behaviours of in situ silica nanoparticle-filled epoxy at different temperatures, Polymer 49 (17) (2008) 3816–3825.
[10] B. Johnsen, A. Kinloch, R. Mohammed, A. Taylor, S. Sprenger, Toughening mechanisms of nanoparticle-modified epoxy polymers, Polymer 48 (2) (2007) 530–541.
[11] B. Wetzel, P. Rosso, F. Haupert, K. Friedrich, Epoxy nanocomposites–fracture and toughening mechanisms, Eng. Fract. Mech. 73 (16) (2006) 2375–2398.
[12] H. Zhang, Z. Zhang, K. Friedrich, C. Eger, Property improvements of in situ epoxy nanocomposites with reduced interparticle distance at high nanosilica content, Acta Mater. 54 (7) (2006) 1833–1842.
[13] J.k. Chen, Z.P. Huang, J. Zhu, Size effect of particles on the damage dissipation in nanocomposites, Compos. Sci. Technol. 67 (14) (2007) 2990–2996.
[14] Y. Huang, A. Kinloch, Modelling of the toughening mechanisms in rubber-modified epoxy polymers. part ii a quantitative description of the microstructure-fracture property relationships, J. Mater. Sci. 27 (10) (1992a) 2763–2769.
[15] T. Hsieh, A. Kinloch, K. Masania, A. Taylor, S. Sprenger, The mechanisms and mechanics of the toughening of epoxy polymers modified with silica nanoparticles, Polymer 51 (26) (2010b) 6284–6294.
[16] P. Dittanet, R.A. Pearson, Effect of bimodal particle size distributions on the toughening mechanisms in silica nanoparticle filled epoxy resin, Polymer 54 (7) (2013) 1832–1845.
[17] D.J. Bray, P. Dittanet, F.J. Guild, A.J. Kinloch, K. Masania, R.A. Pearson, A.C. Taylor, The modelling of the toughening of epoxy polymers via silica nanoparticles: the effects of volume fraction and particle size, Polymer 54 (26) (2013) 7022–7032.
[18] J. Williams, Particle toughening of polymers by plastic void growth, Compos. Sci. Technol. 70 (6) (2010) 885–891.
[19] J. Williams, B. Blackman, H. Steininger, K. Zuo, Toughening by plastic cavitation around cylindrical particles and fibres, Compos. Sci. Technol. 103 (2014) 119–126.
[20] K. Zuo, B. Blackman, J. Williams, H. Steininger, The mechanical behaviour of ZnO nano-particle modified styrene acrylonitrile copolymers, Compos. Sci. Technol. 113 (2015) 9–18.
[21] M. Quaresimin, M. Salviato, M. Zappalorto, A multi-scale and multi-mechanism approach for the fracture toughness assessment of polymer nanocomposites, Compos. Sci. Technol. 91 (2014) 16–21.
[22] K.M. Hamdia, T. Lahmer, T. Nguyen-Thoi, T. Rabczuk, Predicting the fracture toughness of pncs: a stochastic approach based on ANN and ANFIS, Comput. Mater. Sci. 102 (2015a) 304–313.
[23] B. Fisher, M. Ireland, D. Boyland, S. Critten, Why use one model? an approach for encompassing model uncertainty and improving best practice, Environ. Model. Assess. 7 (4) (2002) 291–299.
[24] T. Most, Assessment of structural simulation models by estimating uncertainties due to model selection and model simplification, Comput. Struct. 89 (17) (2011) 1664–1672.
[25] H. Keitel, A. Dimmig-Osburg, L. Vandewalle, L. Schueremans, Selecting creep models using bayesian methods, Mater. Struct. 45 (10) (2012) 1513–1533.
[26] K. Farrell, J.T. Oden, Calibration and validation of coarse-grained models of atomic systems: application to semiconductor manufacturing, Comput. Mech. 54 (1) (2014) 3–19.
[27] E. Prudencio, P. Bauman, D. Faghihi, K. Ravi-Chandar, J. Oden, A computational framework for dynamic data-driven material damage control, based on bayesian inference and model selection, Int. J. Numer. Methods Eng. 102 (3–4) (2015) 379–403.
[28] K.M. Hamdia, M.A. Msekh, M. Silani, N. Vu-Bac, X. Zhuang, T. Nguyen-Thoi, T. Rabczuk, Uncertainty quantification of the fracture properties of polymeric nanocomposites based on phase field modeling, Compos. Struct. 133 (2015b) 1177–1190.
[29] G. Irwin, Analysis of stresses and strains near the end of a crack traversing a plate, J. Appl. Mech. 24 (1957) 361–364.
[30] J. Berriot, F. Lequeux, L. Monnerie, H. Montes, D. Long, P. Sotta, Filler–elastomer interaction in model filled rubbers, a 1 h nmr study, J. Non Cryst. Solids 307 (2002) 719–724.
[31] J. Berriot, F. Martin, H. Montes, L. Monnerie, P. Sotta, Reinforcement of model filled elastomers: characterization of the cross-linking density at the filler–elastomer interface by 1 h nmr measurements, Polymer 44 (5) (2003) 1437–1447.
[32] A. Bansal, H. Yang, C. Li, K. Cho, B.C. Benicewicz, S.K. Kumar, L.S. Schadler, Quantitative equivalence between polymer nanocomposites and thin polymer films, Nat. Mater. 4 (9) (2005) 693–698.
[33] S. Watcharotone, C.D. Wood, R. Friedrich, X. Chen, R. Qiao, K. Putz, L.C. Brinson, Interfacial and substrate effects on local elastic properties of polymers using coupled experiments and modeling of nanoindentation, Adv. Eng. Mater. 13

(5) (2011) 400–404.
[34] G. Odegard, T. Clancy, T. Gates, Modeling of the mechanical properties of nanoparticle/polymer composites, Polymer 46 (2) (2005) 553–562.
[35] R. Qiao, L.C. Brinson, Simulation of interphase percolation and gradients in polymer nanocomposites, Compos. Sci. Technol. 69 (3) (2009) 491–499.
[36] S. Yu, S. Yang, M. Cho, Multi-scale modeling of cross-linked epoxy nanocomposites, Polymer 50 (3) (2009) 945–952.
[37] A. Pontefisso, M. Zappalorto, M. Quaresimin, An efficient RVE formulation for the analysis of the elastic properties of spherical nanoparticle reinforced polymers, Comput. Mater. Sci. 96 (2015) 319–326.
[38] M. Zappalorto, M. Salviato, M. Quaresimin, Influence of the interphase zone on the nanoparticle debonding stress, Compos. Sci. Technol. 72 (1) (2011) 49–55.
[39] M. Zappalorto, M. Salviato, M. Quaresimin, A multiscale model to describe nanocomposite fracture toughness enhancement by the plastic yielding of nanovoids, Compos. Sci. Technol. 72 (14) (2012) 1683–1691.
[40] M. Salviato, M. Zappalorto, M. Quaresimin, Plastic shear bands and fracture toughness improvements of nanoparticle filled polymers: a multiscale analytical model, Compos. Part A Appl. Sci. Manuf. 48 (2013) 144–152.
[41] A. Pontefisso, M. Zappalorto, M. Quaresimin, Influence of interphase and filler distribution on the elastic properties of nanoparticle filled polymers, Mech. Res. Commun. 52 (2013) 92–94.
[42] D.J. MacKay, Bayesian interpolation, Neural Comput. 4 (3) (1992) 415–447.
[43] J.T. Oden, S. Prudhomme, Control of modeling error in calibration and validation processes for predictive stochastic models, Int. J. Numer. Methods Eng. 87 (1–5) (2011) 262–272.
[44] J.L. Beck, K.V. Yuen, Model selection using response measurements: Bayesian probabilistic approach, J. Eng. Mech. (2004).
[45] Y. Huang, A. Kinloch, Modelling of the toughening mechanisms in rubber-modified epoxy polymers. part i finite element analysis studies, J. Mater. Sci. 27 (10) (1992b) 2753–2762.
[46] H. Talebi, M. Silani, T. Rabczuk, Concurrent multiscale modelling of three dimensional crack and dislocation propagation, Adv. Eng. Softw. 80 (2015) 82–92.
[47] H. Talebi, M. Silani, S. Bordas, P. Kerfriden, T. Rabczuk, A computational library for multiscale modelling of material failure,, Comput. Mech. 53 (5) (2014) 1047–1071.
[48] H. Talebi, M. Silani, S.P.A. Bordas, P. Kerfriden, T. Rabczuk, Molecular dynamics/XFEM coupling by a three-dimensional extended bridging domain with applications to dynamic brittle fracture, Int. J. Multiscale Comput. Eng. 11 (6) (2013) 527–541.
[49] P. Budarapu, R. Gracie, S. Bordas, T. Rabczuk, An adaptive multiscale method for quasi-static crack growth, Comput. Mech. 53 (6) (2014) 1129–1148.
[50] P. Budarapu, R. Gracie, Y. Shih-Wei, X. Zhuang, T. Rabczuk, Efficient coarse graining in multiscale modeling of fracture, Theor. Appl. Fract. Mech. 69 (2014) 126–143.